Journal of the Optical Society of America B
OPTICAL PHYSICS

Suppression of self-focusing for few-cycle pulses

Sergei A. Kozlov,[1] Arkadiy A. Drozdov,[1] Saumya Choudhary,[2] Mikhail A. Kniazev,[1] and Robert W. Boyd[2,3,*]

[1]ITMO University, 49 Kronverskiy pr., Saint-Petersburg, 197101, Russia
[2]The Institute of Optics, University of Rochester, Rochester, New York 14627-0186, USA
[3]Department of Physics, University of Ottawa, Ottawa, Ontario K1N6N5, Canada
*Corresponding author: boydrw@mac.com

Received 10 June 2019; revised 11 August 2019; accepted 28 August 2019; posted 29 August 2019 (Doc. ID 369366); published 19 September 2019

Intense beams of light propagating through a medium with a positive Kerr nonlinearity can undergo self-focusing provided that their average power is larger than a certain critical power determined by the wavelength and material properties of the medium. Here, we show that for pulses comprising only a few optical cycles, this self-focusing can be inhibited by the presence of significant (normal) dispersion. We derive simple expressions to quantify the threshold power for self-focusing in the presence of dispersion. In addition, we show that under certain conditions, this threshold power can be larger than conventional critical power (for a dispersionless case) by a factor as large as several hundred.

https://doi.org/10.1364/JOSAB.36.000G68

1. INTRODUCTION

First proposed in 1962 [1], self-focusing is a fundamental self-action effect that occurs when an intense beam of light propagating through a medium with Kerr nonlinearity comes to a focus due to the lensing effect it induces in the medium [2]. Conventionally, the critical power for self-focusing has been derived for a monochromatic (cw) beam by assuming that the diffraction of the beam is compensated for by self-induced focusing [3]. This assumption is valid for optical pulses longer than approximately 1 ns, for which chromatic dispersion has a negligible effect on the temporal form of the pulse as it propagates through the medium [2]. For pulses shorter than a nanosecond, dispersion starts to affect the self-focusing dynamics [4]. For example, even for a pulse that is several optical cycles long, normal (i.e., positive) group velocity dispersion (GVD) can lead to a temporal splitting of the pulse [5,6]. Normal GVD can also increase the self-focusing threshold, or equivalently the critical power, for short pulses, as discussed in [5–8]. In a recent theoretical work, it was shown that the self-focusing process for ultrashort pulses propagating in a dielectric medium is partially suppressed by the increased effect of normal GVD [9]. It was also recently demonstrated [10] that for ultrashort pulses propagating in air, strong normal GVD can even prevent self-focusing from occurring altogether. Further, it was shown [11] that a simple model that ignores any dispersive contributions does not fully explain the observed variation of self-focusing distance with carrier–envelope phase for few-cycle pulses in air.

Essentially, the conventional model of self-focusing based on the concept of a critical power with the usual definition cannot explain the propagation of an intense few-cycle pulse through a nonlinear optical medium. Here, we theoretically study self-action effects in few-cycle optical pulses. We demonstrate that, for few-cycle pulses, the concept of a critical power of self-focusing loses its relevance because of the dominance of dispersion over diffraction. Specifically, dispersion can prevent self-focusing of a few-cycle pulse even when its peak power is larger than the critical power defined in the conventional (cw) sense (or P_{cr}). In addition, we find that for single-cycle pulses, the threshold power for self-focusing can be several hundred times larger than P_{cr}. Our findings are particularly relevant in the context of exploring self-action effects in the terahertz (THz) regime where the conventional high-power sources produce single-cycle pulses [12–15]. Furthermore, the knowledge of the distortion of THz pulses during propagation is important for applications that require the use of single-cycle THz pulses for probing or manipulating material properties [16–18], and for accelerating proton beams [19].

2. THEORY

We assume that a linearly polarized optical pulse propagates along the z axis in an isotropic nonlinear dielectric medium. We describe the electric field in the envelope notation as $E(x, y, z, t) = \mathcal{E}(x, y, z, t)e^{i(k_0 z - \omega_0 t)}$, where $\mathcal{E}$ is the envelope of the electric field, ω_0 is the center angular frequency of the pulse, and $k_0 = n_0\omega_0/c$, where $n_0 = n(\omega_0)$ is the linear refractive index of medium at the central frequency ω_0, and c is the speed of light in vacuum. The pulse propagation through

the medium is modeled by the well-known nonlinear envelope equation (NEE) written in normalized form as [20,21]

$$\frac{\partial\tilde{\mathcal{E}}}{\partial z}+\frac{1}{L_{\mathrm{w}}^{\mathrm{env}}}\frac{\partial\tilde{\mathcal{E}}}{\partial\tilde{t}}+\frac{i}{L_{\mathrm{disp1}}^{\mathrm{env}}}\frac{\partial^2\tilde{\mathcal{E}}}{\partial\tilde{t}^2}-\frac{1}{L_{\mathrm{disp2}}^{\mathrm{env}}}\frac{\partial^3\tilde{\mathcal{E}}}{\partial\tilde{t}^3}$$
$$-\frac{i}{L_{\mathrm{nl1}}^{\mathrm{env}}}\left|\tilde{\mathcal{E}}\right|^2\tilde{\mathcal{E}}+\frac{1}{L_{\mathrm{nl2}}^{\mathrm{env}}}\frac{\partial}{\partial\tilde{t}}\left(\left|\tilde{\mathcal{E}}\right|^2\tilde{\mathcal{E}}\right)=\frac{i}{L_{\mathrm{diffr}}^{\mathrm{env}}}\tilde{\Delta}_{\perp}\tilde{\mathcal{E}}, \quad (1)$$

where $\tilde{\mathcal{E}}=\mathcal{E}/\mathcal{E}_0$ is the normalized envelope of the electric field; $\mathcal{E}_0$ is maximum electric field amplitude at the medium entrance; z represents the coordinate along the direction of beam propagation; $\tilde{t}=t/\tau_0$ is the normalized time, with τ_0 being the pulse width; $\tilde{\Delta}_{\perp}=\partial^2/\partial\tilde{x}^2+\partial^2/\partial\tilde{y}^2$ is the transverse Laplacian operator with $\tilde{x}=x/r_0$, $\tilde{y}=y/r_0$, r_0 being the beam waist radius; $L_{\mathrm{w}}^{\mathrm{env}}=V_g\tau_0$ is the group length, with $V_g=(\partial k/\partial\omega)_{\omega_0}^{-1}$ being the group velocity of the pulse; $L_{\mathrm{disp1}}^{\mathrm{env}}=2\tau_0^2/\beta_2$ and $L_{\mathrm{disp2}}^{\mathrm{env}}=6\tau_0^3/\beta_3$ are the second- and third-order dispersion (TOD) lengths, respectively, where $\beta_2=(\partial^2k/\partial\omega^2)_{\omega_0}$ is the GVD parameter, and $\beta_3=(\partial^3k/\partial\omega^3)_{\omega_0}$ is the TOD parameter, with $k(\omega)=\omega n(\omega)/c$ being the wave number; $L_{\mathrm{nl1}}^{\mathrm{env}}=c/\omega_0\Delta n_{\mathrm{nl}}$ and $L_{\mathrm{nl2}}^{\mathrm{env}}=c\tau_0/\Delta n_{\mathrm{nl}}$ are the nonlinear lengths corresponding to the Kerr contribution and the self-steepening contribution, respectively, and $\Delta n_{\mathrm{nl}}=\frac{1}{2}n_2\mathcal{E}_0^2=n_2'I$ is the intensity-dependent change in refractive index with I being the peak intensity of the input pulse; and $L_{\mathrm{diffr}}^{\mathrm{env}}=2k_0r_0^2$ is the diffraction length. The values of $\tilde{\mathcal{E}}$ and its derivatives in Eq. (1) are of the order of unity. Therefore, the dispersion, nonlinear, and diffraction lengths, as described above, represent the corresponding influences on the propagation of light through the medium.

We note that the inequalities $L_{\mathrm{disp2}}^{\mathrm{env}}>L_{\mathrm{disp1}}^{\mathrm{env}}$ and $L_{\mathrm{nl2}}^{\mathrm{env}}>L_{\mathrm{nl1}}^{\mathrm{env}}$ are valid for multi-cycle optical pulses. Consequently, we will henceforth use $L_{\mathrm{disp1}}^{\mathrm{env}}$ and $L_{\mathrm{nl1}}^{\mathrm{env}}$ to denote the distances at which the shape of the pulse changes noticeably due to dispersion and nonlinearity, respectively.

Let us begin by considering the case

$$L_{\mathrm{nl1}}^{\mathrm{env}}=L_{\mathrm{diffr}}^{\mathrm{env}}, \quad (2)$$

i.e., the situation in which nonlinear and diffractive effects are equally important. This situation corresponds to the conventional critical power for self-focusing, and by introducing the expressions for $L_{\mathrm{nl1}}^{\mathrm{env}}$ and $L_{\mathrm{diffr}}^{\mathrm{env}}$ and the expression $P=(\pi r_0^2)I$, we find that

$$P_{\mathrm{cr}}=R_{\mathrm{cr}}\frac{\lambda_0^2}{8\pi n_0n_2'}, \quad (3)$$

where R_{cr} is a parameter whose value depends on the input beam profile [22,23], and $\lambda_0=2\pi/k_0$ is the central wavelength of radiation. For an axially symmetric collimated Gaussian beam, $R_{\mathrm{cr}}=3.77$ [22,23]. The situation given in (2) corresponds to the case where $R_{\mathrm{cr}}=1$. We will, however, use $R_{\mathrm{cr}}=3.77$ in the subsequent calculations of P_{cr}.

We next consider the situation given by

$$L_{\mathrm{disp1}}^{\mathrm{env}}<L_{\mathrm{diffr}}^{\mathrm{env}}. \quad (4)$$

We note that in this case, the nonlinearity competes with GVD instead of diffraction. Under these conditions, the concept of P_{cr}, as defined in (3), begins to lose its meaning. The inequality (4) can be rewritten as

$$\frac{l_0}{D_0}<\sqrt{c\omega_0n(\omega_0)\beta_2}, \quad (5)$$

where $l_0=2c\tau_0$ is the longitudinal extent of the pulse (or wave packet), and $D_0=2r_0$ is its transverse size. We consider the form of dispersion to be given by

$$n(\omega)=N_0+ac\omega^2, \quad (6)$$

where empirical parameters N_0 and a characterize the medium dispersion. We then rewrite the inequality (5) as

$$\frac{l_0}{D_0}<\sqrt{6N_0\Delta n_{\mathrm{disp}}}, \quad (7)$$

where $\Delta n_{\mathrm{disp}}=ac\omega_0^2$ is the modification of the refractive index at the central wavelength due to dispersion. To derive inequality (7), we have considered that usually $\Delta n_{\mathrm{disp}}\ll N_0$. Specifically for the examples that we have discussed in the next section, Δn_{disp} is 2.634×10^{-2} and N_0 is 4.7344 for the THz pulses, while Δn_{disp} is 2.433×10^{-3} and N_0 is 1.4508 for the near-infrared (IR) pulses, where $\Delta n_{\mathrm{disp}}=ac\omega^2-bc/\omega^2$. One can therefore expect that for wave packets with longitudinal dimension less than the transverse size (or "light pancakes"), the concept of critical power for self-focusing would lose its physical meaning.

3. NUMERICAL MODELING

In this section, we numerically study the changes in self-action phenomena under the conditions (5) and (7) for two typical cases. For the first case, we consider a pulse with $\lambda_0=800$ nm that propagates through bulk fused silica, which is normally dispersive in the assumed spectral region with a dispersion relation given by

$$n(\omega)=N_0+ac\omega^2-bc/\omega^2, \quad (8)$$

where $N_0=1.4508$, $a=2.7401\cdot10^{-44}$ s^3/cm, and $b=3.9437\cdot10^{17}1/(\mathrm{s}\cdot\mathrm{cm})$ [24]. Here, the condition (5) becomes $l_0/D_0>0.18$. For the second case, we consider a pulse with $\nu_0=c/\lambda_0=1.0$ THz that propagates through a normally dispersive stoichiometric MgO:LiNbO$_3$ crystal, whose dispersion relation is given by (6), where $N_0=4.734$ and $a=2.224\cdot10^{-38}$ s^3/cm [25]. In this case, the condition (7) becomes $l_0/D_0>0.87$. In both cases, we consider pulses with fewer than 10 oscillations of the optical field. Assuming cylindrical symmetry, we write the electric field at the entrance of the medium (or at $z=0$) in the envelope notation as

$$E(0,r,t)=\mathcal{E}(0,r,t)\sin(\omega_0t), \quad (9)$$

where the envelope $\mathcal{E}$ is assumed to have Gaussian transverse and temporal profiles, i.e.,

$$\mathcal{E}(0,r,t)=\mathcal{E}_0\exp\left(-\frac{r^2}{{r_0}^2}\right)\exp\left(-\frac{t^2}{{\tau_0}^2}\right), \quad (10)$$

with $r=\sqrt{x^2+y^2}$ being the radial coordinate.

In our numerical simulations, we use the following normalized form of Eq. (10):

$$\tilde{\mathcal{E}}\left(0,\tilde{r},\tilde{t}\right)=\exp\left(-\tilde{r}^2\right)\exp\left(-\tilde{t}^2\right). \tag{11}$$

In all cases, we assume that the peak power of the pulse P_0 is larger than P_{cr}. Since we are considering the evolution of pulses that are at most a few cycles in duration, we treat the evolution of the full electric field of the pulse $E(0,r,t)$, and not just its envelope $\mathcal{E}(0,r,t)$ [24,26]. Hence, instead of the NEE shown in (1), we consider the following carrier-resolved propagation equation written in the normalized form:

$$\frac{\partial\tilde{E}}{\partial z}+\frac{1}{L^{f}_{wave}}\frac{\partial\tilde{E}}{\partial\tilde{t}}-\frac{1}{L^{f}_{disp1}}\frac{\partial^3\tilde{E}}{\partial\tilde{t}^3}+\frac{1}{L^{f}_{disp2}}\int_{-\infty}^{\tilde{t}}\tilde{E}d\tilde{t}'+\frac{1}{L^{f}_{nl}}\tilde{E}^2\frac{\partial\tilde{E}}{\partial\tilde{t}}=\frac{1}{L^{f}_{diffr}}\tilde{\Delta}_{\perp}\int_{-\infty}^{\tilde{t}}\tilde{E}d\tilde{t}', \tag{12}$$

where $\tilde{E}=E/E_0$ is the normalized electric field amplitude, E_0 is the maximum electric field amplitude at the entrance to the nonlinear medium, $\tilde{t}=t/\tau_0$ is the normalized time, $\tilde{x}=x/r_0$, $\tilde{y}=y/r_0$, $L^{f}_{wave}=c/N_0\omega_0$, $L^{f}_{nl}=(1/4)L^{env}_{nl1}$, $L^{f}_{diffr}=L^{env}_{diffr}$,

$$\left[L^{f}_{disp1}\right]^{-1}=\frac{(\omega_0\tau_0)^2}{4}\left(\frac{1}{L^{env}_{disp1}}+\frac{\omega_0\tau_0}{L^{env}_{disp2}}\right), \tag{13}$$

and

$$\left[L^{f}_{disp2}\right]^{-1}=-\frac{(\omega_0\tau_0)^2}{4}\left(\frac{1}{L^{env}_{disp1}}-3\frac{\omega_0\tau_0}{L^{env}_{disp2}}\right). \tag{14}$$

Appendix A has the detailed derivation of the NEE from the unnormalized carrier-resolved propagation equation.

The generalized field equation (12), which can be rewritten as Eq. (1) for the special case of quasi-monochromatic pulses (see Appendix A), correctly describes the dynamics of the self-focusing process including spectral broadening and the generation of radiation at odd harmonics of the input frequency [25]. We use the split-step Fourier method for the numerical integration of (12) [21]. The effects of dispersion and diffraction are calculated in the spectral domain, while the effect of nonlinearity is calculated in the time domain by the Crank–Nicolson method. The fast Fourier transform algorithm is used to transform from the spectral to the temporal domain, and vice versa. We first study the propagation of a multi-cycle pulse through a normally dispersive medium. Here, we discuss only the propagation of a near-IR pulse propagating through fused silica ($n_2'=2.9\times10^{-16}$ cm^2/W [24]). We assume $\lambda_0=800$ nm, intensity $I=5\times10^{11}$ W/cm^2, and beam radius $r_0=30\lambda_0$, which corresponds to $L^{env}_{diffr}=13$ mm, at the entrance to the medium. The critical power for self-focusing P_{cr} obtained from (3) is 2.3×10^6 W for the parameters considered and is consistent with the known value [27]. We assume a pulse width of $\tau_0=27$ fs, which corresponds to an l_0/D_0 ratio of 0.3 (or $L^{env}_{disp1}=3.3L^{env}_{diffr}$. We also assume the number N of oscillations of the optical field ($N=2\tau_0/T_0$, where $T_0=2\pi/\omega_0$) at the entrance to medium is $N=20$. The peak power of the input pulse P_0 is taken to be $4P_{cr}$. Figure 1 shows the spatiotemporal evolution of the aforementioned fs pulse as it propagates through the medium. The panels in the left column of the figure depict two-dimensional density plots of the pulse at different distances (z) within the medium. The panels in the right column show the modulus of the field spectrum on the beam axis ($r=0$) for the corresponding distances, i.e., they show $G(z,0,\omega)$, which is obtained from the following Fourier transform relation:

$$G(z,0,\omega)=\int_{-\infty}^{+\infty}E(z,0,t)\exp(-i\omega t)\,dt. \tag{15}$$

The insets in panels in the right column of the figure show the corresponding modulus of the electric field $|E(z,0,t)|$ on the beam axis.

As seen in the left panel of Fig. 1(a), the pulse initially undergoes transverse as well as longitudinal compression leading to the formation of a self-focused filament at $\tilde{z}=z/L^{env}_{diffr}=0.2$ [left, Fig. 1(b)]. Here, the peak intensity of the pulse increases by a factor of 6.6, while the pulse width (spectral width) decreases (increases) by a factor of 1.4 (2.7). Also, the maximum of the spectrum red-shifts, while the blue region of the spectrum undergoes a larger broadening. Noticeable radiation is generated at tripled frequencies. Our estimates of the nonlinearity, diffraction, and dispersion lengths for the pulse at $\tilde{z}=0.2$ (or $z=2.5$ mm) are: $L^{env}_{nl1}=0.1$ mm, $L^{env}_{nl2}=5.9$ mm, $L^{env}_{diffr}=0.8$ mm, and $L^{env}_{disp1}=22$ mm. In other words, the main influence on the nature of optical wave propagation is exerted by the Kerr nonlinearity. The effect of intensity-dependent group velocity, which leads to self-steepening, becomes evident in Fig. 1(c), where the trailing edge of the pulse envelope [inset, right column, Fig. 1(c)] becomes more pronounced than the leading edge. Linear effects (dispersion and diffraction) start to dominate from a distance $\tilde{z}=0.25$ (or $z=3.3$ mm) onwards causing the pulse to spread spatiotemporally, which lowers the intensity at the center of the pulse causing it to split temporally [inset, right column, Fig. 1(d)]. This observed spectral and temporal evolution is consistent with previously reported experimental findings for ultrashort pulses propagating in a nonlinear medium, and serves to verify our numerical integration procedure [28]. A more detailed theoretical analysis of this particular case can also be found in [29]. A multi-cycle THz pulse shows very similar qualitative behavior as it propagates through a MgO : $LiNbO_3$ crystal (see Appendix B for the corresponding plots).

A. Near-IR Radiation

Figure 2 shows the spatiotemporal evolution of a shorter ($\tau_0=8$ fs) near-IR (800 nm) pulse, which corresponds to an l_0/D_0 ratio of 0.1 (or $L^{env}_{disp1}=0.3L^{env}_{diffr}$, and $N=6$ at the entrance to medium as it propagates through fused silica. All the other parameters are taken to be the same as the multi-cycle near-IR pulse shown in Fig. 1. As seen in the left panels of Figs. 2(b) and 2(c), there is no transverse compression (self-focusing) of the pulse. Instead, significant temporal spreading of the pulse occurs due to the strong dispersion even for distances as small as $\tilde{z}=0.11$ (or $z=1.5$ mm). As a result, the peak intensity of the pulse is uniformly reduced, thereby decreasing the Kerr contributions as well and arresting the process of self-focusing. The third-order

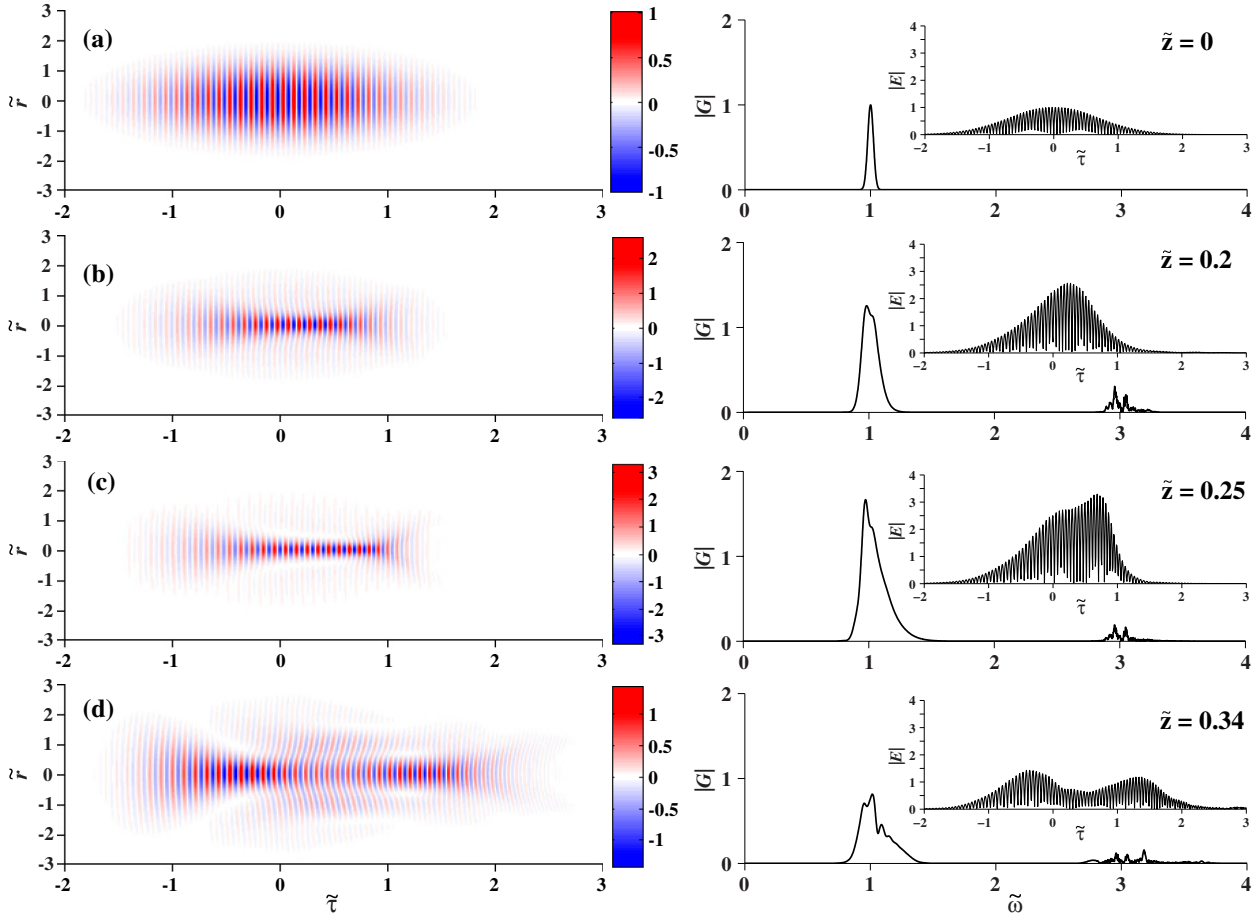

Fig. 1. Left: spatiotemporal evolution of the electric field amplitude E of a near-IR pulse propagating through fused silica. Right: modulus $|G|$ of the frequency spectrum on the beam axis for the same propagation distances $\tilde{z}$, with the time-varying field $|E|$ in the insets. The parameters of the input pulse are: $\lambda_0 = 800$ nm, $r_0 = 30\lambda_0$, $\tau_0 = 27$ fs (i.e., $N = 20$), $I = 5 \times 10^{11}$ W/cm^2. Here, $\tau = t - z/V_g$ is the retarded time, $\tilde{r} = r/r_0$, $\tilde{\tau} = \tau/\tau_0$, $\tilde{\omega} = \omega/\omega_0$. We see that self-focusing dynamics is not appreciably influenced by pulse duration effects under the conditions reported here. The spatiotemporal evolution shown here is consistent with reported results [5,6,9,28].

nonlinearity of the medium gives rise to a slight broadening of the spectrum and noticeable generation of radiation at third-harmonic frequencies [right, Figs. 2(b) and 2(c)].

B. THz Radiation

The value of n_2 of materials at THz frequencies can be several orders of magnitude larger than the corresponding value of n_2 at visible and near-IR frequencies [30–32]. In recent years, there have been several works on the measurement of n_2 of various materials at THz frequencies [31–34]. It is important to note that the typical methods for measuring n_2 of quasi-monochromatic pulses in the visible and near-IR spectral ranges can give significant methodological errors for few-cycle pulses, which become especially significant for the single-cycle pulses produced by conventional THz sources [34]. In [31], Korpa *et al.* have used an alternative technique to estimate the approximate value of the nonlinear refractive index of lithium niobate ($LiNbO_3$) at THz frequencies by comparing the result of the measurement of transmitted time-varying electric field through the sample given in [35] with their numerical simulations. Due to the limitations of available pulse intensities and crystal lengths, Korpa *et al.* [31] are able to provide an order-of-magnitude estimate of the n_2 of $LiNbO_3$ at THz frequencies, which is three orders of magnitude larger than the value at visible frequencies in concurrence with the earlier similar theoretical predictions [30]. In addition, Korpa *et al.* have numerically demonstrated the influence of diffraction on the propagation of few-cycle, near-IR pulses in fused silica. However, they have not performed a rigorous study of the self-focusing dynamics of these few-cycle pulses [31].

We now study the propagation of single-cycle THz pulses through a stoichiometric MgO:$LiNbO_3$ crystal with nonlinear refractive index $n_2' = 5.4 \times 10^{-12}$ cm^2/W [35] and dispersion parameters described at the beginning of Section 3. It should be noted that we have used an earlier reported value of n_2 of the MgO:$LiNbO_3$ crystal [35], which might not be accurate due to the aforementioned methodological errors in measurement of n_2 in the THz region. However, our calculations have been performed with normalized parameters, and it is straightforward to extend our results if further experiments refine the value of n_2 by changing the electric field intensity so as to have the same value of Δn_{nl} considered here.

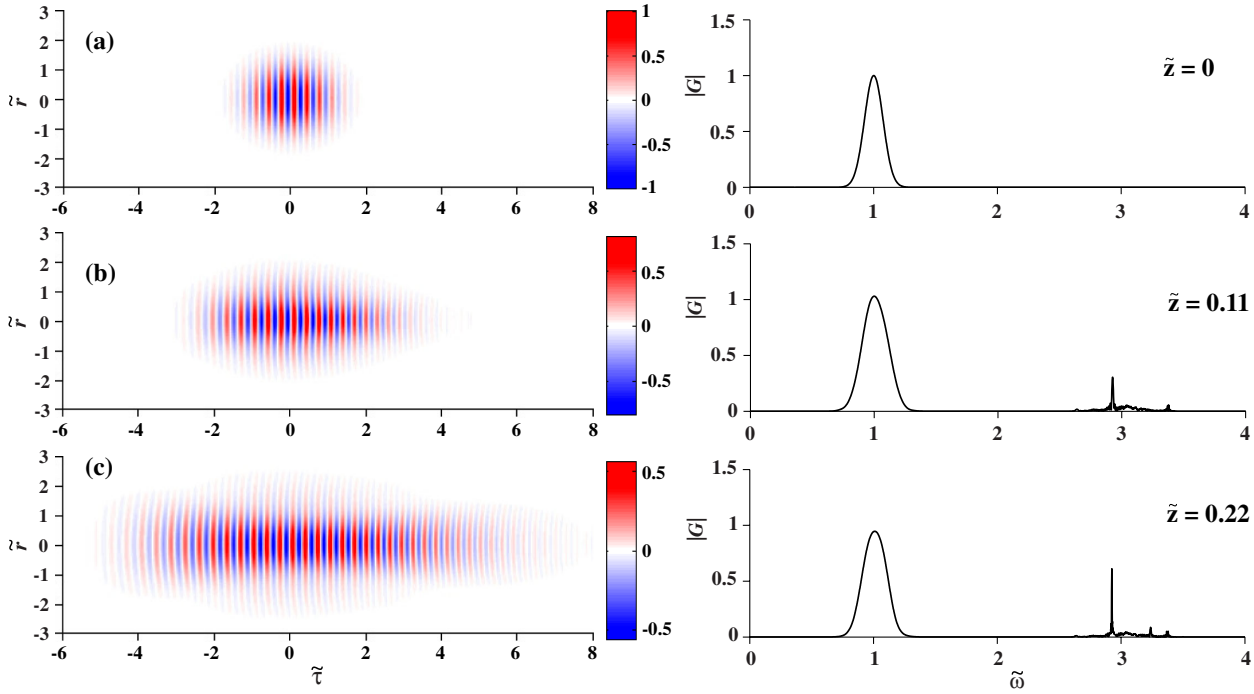

Fig. 2. Left: spatiotemporal evolution of the electric field amplitude E of a near-IR few-cycle pulse propagating through fused silica. Right: modulus $|G|$ of the frequency spectrum on the beam axis for the same propagation distances $\tilde{z}$. The parameters of the input pulse are: $\lambda_0 = 800$ nm, $r_0 = 30\lambda_0$, $\tau_0 = 8$ fs (i.e., $N = 6$), and $I = 5 \times 10^{11}$ W/cm^2, corresponding to $P = 4P_{cr}$. Instead of transverse and longitudinal compression of the pulse as observed in Figs. 1(b) and 1(c), here, we observe significant temporal broadening due to the strong GVD, but no transverse compression (i.e., no self-focusing). We see that, for this few-cycle optical pulse, the strong normal GVD is able to inhibit self-focusing even though $P = 4P_{cr}$.

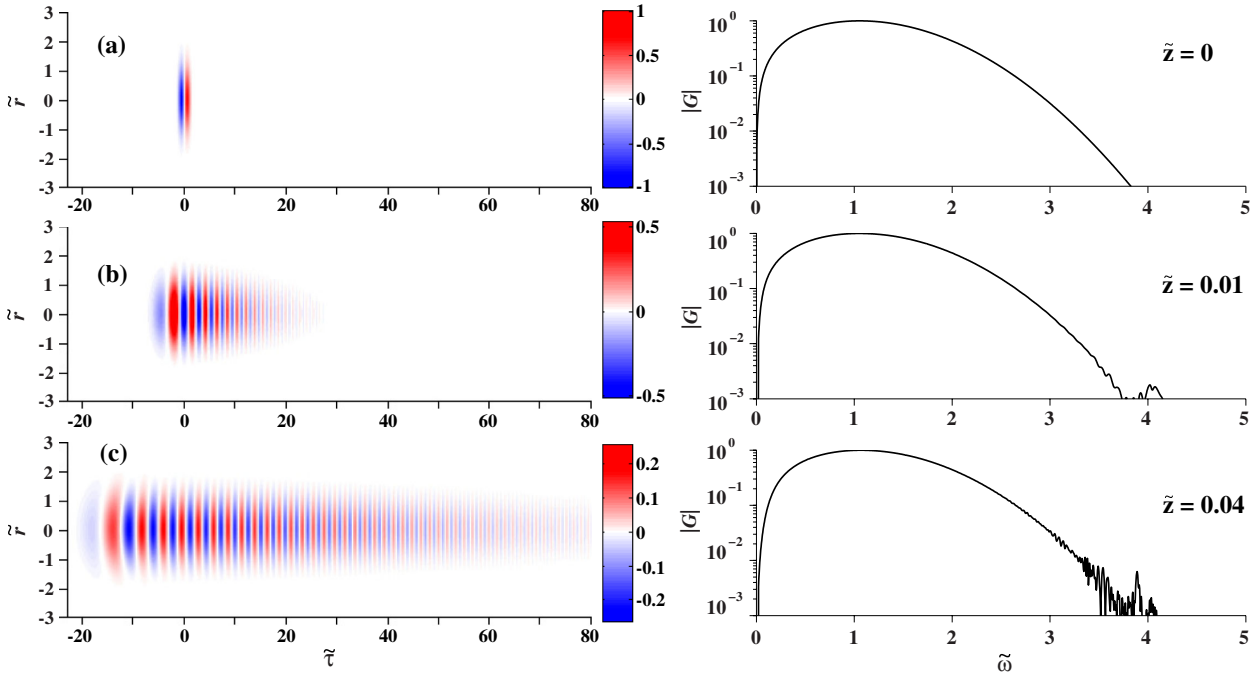

Fig. 3. Left: spatiotemporal evolution of the electric field amplitude E of a single-cycle THz pulse propagating in a MgO : $LiNbO_3$ crystal. Right: modulus $|G|$ of the frequency spectrum on the beam axis for the same propagation distances $\tilde{z}$. The parameters of the input pulse are: $\lambda_0 = 300$ μm, $r_0 = 5\lambda_0$, $\tau_0 = 0.3$ ps (i.e., $N = 0.6$), and $I = 3 \times 10^8$ W/cm^2 corresponding to $P = 4P_{cr}$. For the single-cycle THz pulse considered here, we again see that the strong dispersive spreading of the pulse overcomes self-focusing even for $P = 4P_{cr}$, and dominates the evolution of the pulse as it propagates through the medium.

We assume pulses with $\lambda_0 = 300\ \mu m$, a peak electric field amplitude $\mathcal{E}_0 = 0.2$ MV/cm (or peak intensity $I_0 = \frac{1}{2} n_0 \epsilon_0 c_0 |\mathcal{E}_0|^2 = 3 \times 10^8$ W/cm^2, with ϵ_0 being the vacuum permittivity), and beam radius $r_0 = 5\lambda_0$, which corresponds to $L_{\text{diffr}}^{\text{env}} = 45$ cm, at the entrance to the medium. The critical power for self-focusing, P_{cr}, for this case is 5.3×10^6 W. The pulse width is taken to be $\tau_0 = 0.3$ ps (shown in Fig. 3), which corresponds to an l_0/D_0 ratio of 0.06 (or $L_{\text{disp1}}^{\text{env}} = 4.8 \times 10^{-3} L_{\text{diffr}}^{\text{env}}$, and $N = 0.6$). The peak power of the input pulse P_0 is $4P_{\text{cr}}$, as in the previous case.

Figure 3 shows the spatiotemporal evolution of the single-cycle THz pulse. The strong dispersion is evidenced by the

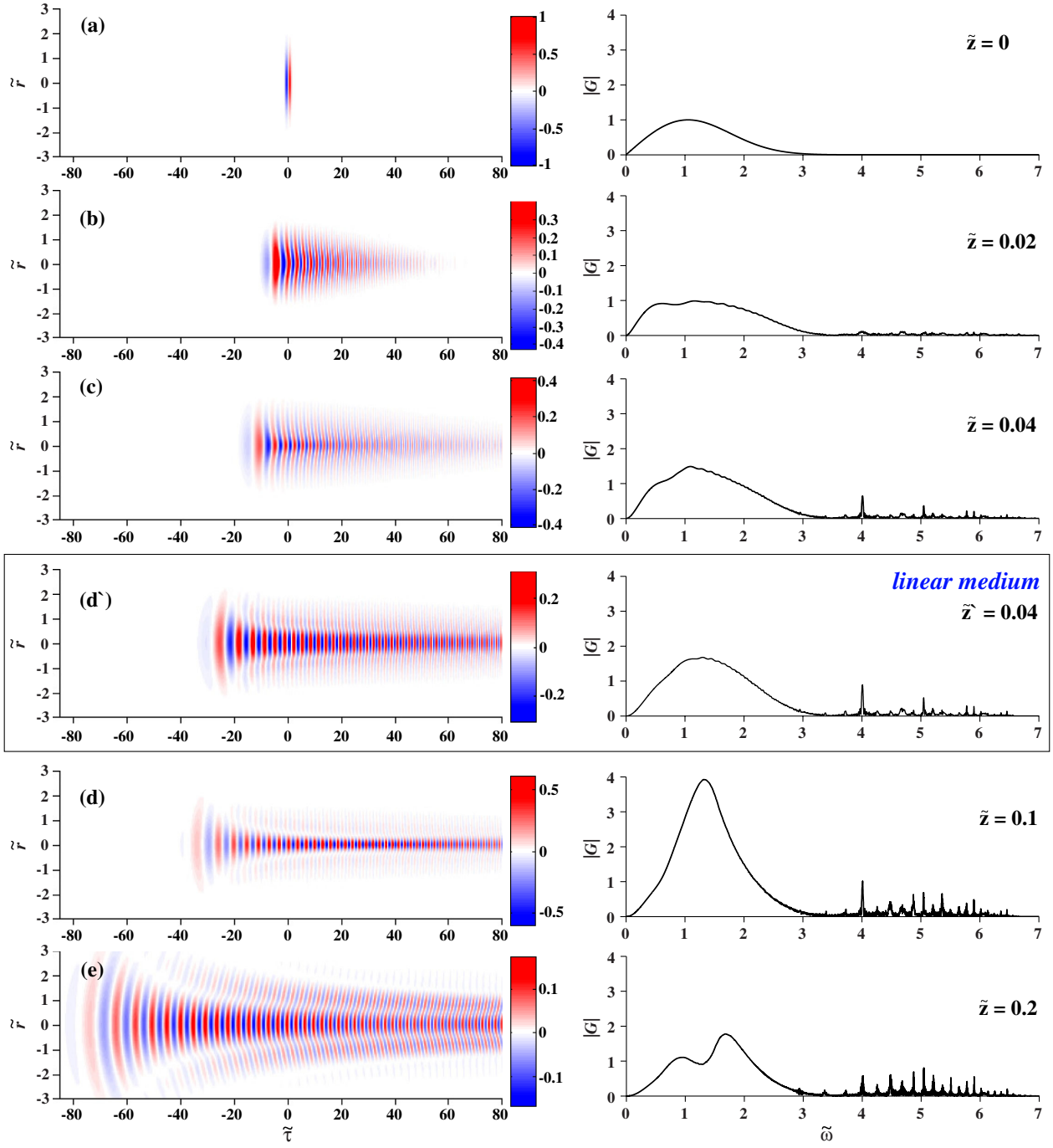

Fig. 4. Left: spatiotemporal evolution of the electric field amplitude E of a very intense, single-cycle THz pulse propagating in a MgO:LiNbO$_3$ crystal. Right: modulus $|G|$ of the frequency spectrum on the beam axis for the same propagation distances $\tilde{z}$. The parameters of the input pulse are: $\lambda_0 = 300\ \mu m$, $r_0 = 5\lambda_0$, $\tau_0 = 0.3$ ps, $I = 1.48 \times 10^{10}$ W/cm^2, corresponding to $P = 200 P_{\text{cr}}$. The panel (d') shows the output of propagating the pulse in the left panel of (c) through the entire length of the medium while considering only linear propagation, or equivalently with the nonlinear contributions neglected ($n_2' = 0$). In contrast with the spatiotemporal evolution of a single-cycle THz pulse for $P = 4P_{\text{cr}}$ shown in Fig. 3, here, we find that transverse compression (self-focusing) does occur. We observe self-focusing of the pulse [left, panels (c) and (d)] followed by dispersive-diffractive spreading of the pulse with further propagation [left, panel (e)].

significant temporal broadening of the pulse for propagation distances as small as $\tilde{z} = 0.01$ (or $z = 0.5$ cm), seen in the left panel (b). Also, as observed in the subsequent panel, there is no transverse compression of the pulse, or self-focusing, for the propagation distances considered. We note that the maximum propagation distance considered here is 0.04 (or $z = 2$ cm), which is an order of magnitude larger than the dispersion length L_{disp1} for this case. The third-order nonlinearity manifests in the negative (positive) chirp of the leading (trailing) edge of the pulse [left, Figs. 3(b) and 3(c)], and the generation of new frequency components in the blue region of the spectrum [right, Figs. 3(b) and 3(c)] due to the Kerr effect. The effect of diffraction is present only in the leading edge of the pulse, as indicated by the curvature of the wavefront at the leading edge of the pulse [left, Figs. 3(b) and 3(c)]. This temporal asymmetry in diffraction is due to the fact that lower-frequency spectral components on the leading edge of the pulse diffract more strongly than the higher-frequency components on the trailing edge of the pulse.

We further examine the spatiotemporal evolution of a single-cycle THz pulse ($\tau_0 = 0.3$ ps) with a significantly larger peak power at the input. Specifically, we consider the situation where $P_0/P_{\text{cr}} = 200$, which corresponds to a peak electric field amplitude of $\mathcal{E}_0 = 1.53$ MV/cm (or peak intensity $I_0 = 1.48 \times 10^{10}$ W/cm^2). Here, we do observe self-focusing, as evidenced in the left panels of Figs. 4(d) and 4(e). However, in contrast to the case considered in Fig. 1, the pulse undergoes significant temporal broadening due to both strong dispersion and large nonlinearity. The temporal broadening is even larger than in Fig. 3 (where $P_0/P_{\text{cr}} = 4$) due to the significantly larger nonlinear contribution. We note that the Kerr effect is also manifested by the significant wavefront curvature at the steeper leading edge of the pulse prior to self-focusing [Figs. 4(b) and 4(c)]. This curvature leads to self-focusing upon further propagation and the formation of a self-trapped filament at the distance of $\tilde{z} = 0.1$ (or $z = 4.4$ cm) [Fig. 4(d)]. Figure 4(d') additionally shows the result of propagation of the pulse in the left panel of Fig. 4(c) in the same medium while ignoring the nonlinear contributions ($n_2' = 0$). As can be seen clearly in Fig. 4(d'), the self-focusing occurs even for linear propagation due to the large wavefront curvature. In addition, significant generation of radiation is observed at the odd harmonics along with a gradual blue-shift of the maximum of the spectral density [Figs. 4(c)–4(e)]. Subsequently, the usual dispersive-diffraction spreading of the pulse continues after the formation of the filament [Fig. 4(e)].

4. CONCLUSION

To summarize, through the use of an inequality [expression (5)] that compares the geometric parameters of an optical pulse (specifically, the ratio of its longitudinal dimension to its transverse dimension) propagating in a nonlinear medium, with the material parameters of the medium, we have identified a regime in which the concept of a critical power for self-focusing loses its validity. In this regime, self-focusing of intense few-cycle pulses is arrested even for peak powers larger than the critical power because of the predominance of dispersion over diffraction that competes with nonlinear refraction. We have numerically confirmed the validity of this prediction for two different cases of ultrashort pulse propagation in nonlinear media, with the first case being a near-IR pulse and the second being a THz pulse. We have further shown that for single-cycle pulses, the critical power for self-focusing can increase by two orders of magnitude. Due to this significant nonlinear contribution, a single-cycle pulse evolves differently in comparison with few-cycle pulses that undergo self-focusing. Furthermore, the suppression of self-focusing of single-cycle pulses for powers that are achievable in practice also implies that the possibility of optical damage would be significantly reduced.

APPENDIX A: DERIVATION OF THE NONLINEAR ENVELOPE EQUATION FROM THE CARRIER-RESOLVED PULSE PROPAGATION EQUATION

The dynamics of the electric field E of a paraxial linearly polarized wave propagating in an isotropic dispersive medium with a linear refractive index given by Eq. (8), and an instantaneous (or inertia-less) cubic non-linearity characterized by the coefficient of nonlinear refractive index n_2 has the form [24,26]

$$\frac{\partial E}{\partial z} + \frac{N_0}{c}\frac{\partial E}{\partial t} - a\frac{\partial^3 E}{\partial t^3} + b\int_{-\infty}^{t} E\,dt' + gE^2\frac{\partial E}{\partial t} = \frac{c}{2N_0}\Delta_\perp \int_{-\infty}^{t} E\,dt', \tag{A1}$$

where $g = 3n_2/c$ [26]. Equation (12) was obtained from Eq. (A1) through the use of normalization factors given in Eqs. (13) and (14). This normalized carrier-resolved pulse propagation equation was subsequently used in our numerical simulations.

The nonlinear envelope equation, given by Eq. (1), is a special case of Eq. (A1) that is applicable in the regime where the envelope approximation of the field is valid. This regime includes the well-known case of quasi-monochromatic pulses [21], as well as the cases where there is at least one complete optical cycle within the full-width at half-maximum pulse width [20,36]. To derive Eq. (1) from Eq. (A1), following the steps outlined in [24], we make the following substitution for the electric field in (A1):

$$E(\mathbf{r}, t) = \frac{1}{2}\mathcal{E}(\mathbf{r}, t)^{i(k_0 z - \omega_0 t)} + \text{c.c.} \tag{A2}$$

Here, ω_0 is an arbitrary fixed frequency, $k_0 (= \omega_0 n(\omega_0)/c)$ is the corresponding propagation constant, with $n(\omega)$ being the linear refractive index described by Eq. (6) or (8), and $\mathcal{E}(\mathbf{r}, t)$ is a new variable that represents a slowly evolving field envelope. The time derivatives on the left-hand side of Eq. (A1) are straightforward to calculate after substituting the electric field given by (A2) in (A1). In the calculation of the integral on the left-hand side, repeated integration by parts would result in a power series in $(i/\omega_0)^n$ with the corresponding coefficients being $\partial^n \mathcal{E}/\partial t^n$. We subsequently make the unidirectional approximation and consider only the forward-propagating components in (A1), which gives us the following equation in the envelope notation after some simplification:

$$\frac{\partial \mathcal{E}}{\partial z}+\frac{1}{V}\frac{\partial \mathcal{E}}{\partial t}+i\frac{\beta_2}{2}\frac{\partial^2 \mathcal{E}}{\partial t^2}-\frac{\beta_3}{6}\frac{\partial^3 \mathcal{E}}{\partial t^3}$$
$$-\sum_{n=4}^{\infty}\beta_n\frac{i^{n+1}}{n!}\frac{\partial^n \mathcal{E}}{\partial t^n}-i\gamma_1|\mathcal{E}|^2\mathcal{E}+\gamma_2\frac{\partial}{\partial t}\left(|\mathcal{E}|^2\mathcal{E}\right)$$
$$-\left(i\gamma_1\mathcal{E}^3-\gamma_2\mathcal{E}^2\frac{\partial \mathcal{E}}{\partial t}\right)\exp\left(2i(k_0z-\omega_0t)\right)$$
$$=\frac{i}{2k_0}\Delta_\perp\left[\frac{\omega_0}{i}\int_{-\infty}^{t}\mathcal{E}(\mathbf{r},t')\exp\left(i\omega_0(t-t')\right)dt'\right], \tag{A3}$$

where $V=(\frac{\partial k}{\partial \omega})^{-1}_{\omega_0}$, $\beta_n=(\frac{\partial^n k(\omega)}{\partial \omega^n})_{\omega_0}$, $k=\frac{N_0}{c}\omega+a\omega^3-\frac{b}{\omega}$, $\gamma_1=\frac{g\omega_0}{4}$, $\gamma_2=\frac{g}{4}$.

For quasi-monochromatic pulses, it can be assumed that ω_0 is equal to the carrier frequency, and the variable $\mathcal{E}(\mathbf{r},t)$ can then be associated with the envelope of the pulse. We now consider dispersion terms only until the third order, which requires neglecting the summation term on the left-hand side of Eq. (A3). We also ignore the last term on the left-hand side, which describes the generation of harmonics. The diffraction term on the right-hand side is expanded as follows [29]:

$$\frac{i}{2k_0}\Delta_\perp\left[\frac{\omega_0}{i}\int_{-\infty}^{t}\mathcal{E}(\mathbf{r},t')\exp\left(i\omega_0(t-t')\right)dt'\right]$$
$$=\frac{i}{2k_0}\Delta_\perp\left(\mathcal{E}(\mathbf{r},t)-\frac{i}{\omega_0}\frac{\partial \mathcal{E}(\mathbf{r},t)}{\partial t}+\left(\frac{i}{\omega_0}\right)^2\frac{\partial^2 \mathcal{E}(\mathbf{r},t)}{\partial t^2}-\ldots\right), \tag{A4}$$

with the result on the right obtained by integration by parts. We include only the first term of this expansion in (A3) to obtain the well-known nonlinear envelope equation [21]

$$\frac{\partial \mathcal{E}}{\partial z}+\frac{1}{V}\frac{\partial \mathcal{E}}{\partial t}+i\frac{\beta_2}{2}\frac{\partial^2 \mathcal{E}}{\partial t^2}-\frac{\beta_3}{6}\frac{\partial^3 \mathcal{E}}{\partial t^3}-i\gamma_1|\mathcal{E}|^2\mathcal{E}$$
$$+\gamma_2\frac{\partial}{\partial t}\left(|\mathcal{E}|^2\mathcal{E}\right)=\frac{i}{2k_0}\Delta_\perp\mathcal{E}. \tag{A5}$$

For few-cycle pulses, which have a broad spectrum, the number of dispersion terms considered in the envelope equation can be increased in order to adequately describe the dependence of $k(\omega)$ throughout the pulse spectra. The corresponding integral terms on the right-hand side that describe diffraction should

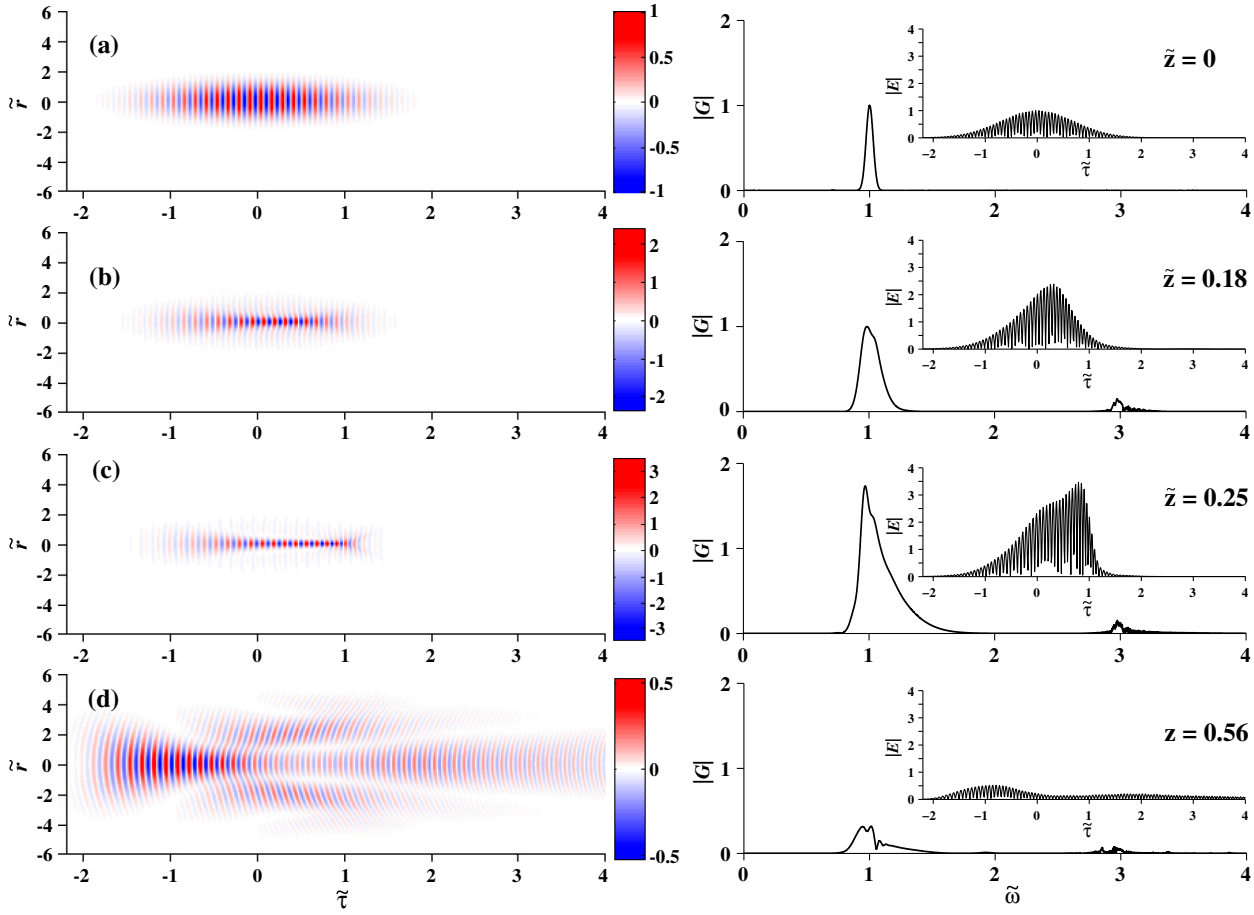

Fig. 5. Left: spatiotemporal evolution of the electric field amplitude E of the few-cycle THz pulse propagating in a MgO:LiNbO$_3$ crystal. Right: modulus $|G|$ of the frequency spectrum on the beam axis for the same propagation distances $\tilde{z}$, with the time-varying field $|E|$ in the insets. The parameters of the input pulse are: $\lambda_0=300$ μm, $r_0=5\lambda_0$, $\tau_0=8$ ps (i.e., $N=16$), $I=3\times10^8$ W/cm^2, and $P_0=4P_{cr}$, where $P_{cr}=5.3\times10^6 W$. For the multiple-optical-cycles-long THz pulse shown here, the spatial evolution of the pulse is functionally similar to the evolution of multi-cycle near-IR pulses propagating in a normally dispersive medium, shown in Fig. 1.

also be included. We note that in reference [20], this term is written in the form of an equivalent inverse operator:

$$\frac{\omega_0}{i}\int_{-\infty}^{t}\mathcal{E}(r,z,t')\exp\left(i\omega_0(t-t')\right)dt'=\left[1+\frac{i}{\omega_0}\frac{\partial}{\partial t}\right]^{-1}\times\mathcal{E}(r,z,t). \tag{A6}$$

The validity of the representation (A6) can be easily verified by applying the operator $\left[1+\frac{i}{\omega_0}\frac{\partial}{\partial t}\right]$ to both the left- and the right-hand sides of Eq. (A6).

Equation (A5) above when written in the normalized form gives Eq. (1). The normalizing factors and their implications are discussed at length in Section 2. The same normalization factors can be used to rewrite Eq. (A1) as Eq. (12).

APPENDIX B: SPATIOTEMPORAL EVOLUTION OF A MULTI-CYCLE THZ PULSE THROUGH A NORMALLY DISPERSIVE MEDIUM

Here, we treat the spatiotemporal dynamics of a multi-cycle THz pulse as it propagates through the normally dispersive MgO:$LiNbO_3$ crystal ($n_2' = 5.4\times10^{-12}\,\mathrm{cm^2/W}$) [35] and dispersion parameters described at the beginning of Section 3 in the main text. We also note that at present, the generation of multi-cycle THz waveforms with high intensity is a big challenge [37–39].

We assume a pulse with $\lambda_0 = 300\,\mu\mathrm{m}$, intensity $I = 3\times10^8\,\mathrm{W/cm^2}$ (or amplitude 0.2 MV/cm), and beam radius $r_0 = 5\lambda_0$, which corresponds to $L_{\mathrm{diffr}}^{\mathrm{env}} = 45\,\mathrm{cm}$, at the entrance to the medium. The critical power for self-focusing, P_{cr}, for this case is 5.3×10^6 W. The pulse width is assumed to be $\tau_0 = 8$ ps, which corresponds to an l_0/D_0 ratio of 1.6 (or $L_{\mathrm{disp1}}^{\mathrm{env}} = 3.4L_{\mathrm{diffr}}^{\mathrm{env}}$). The peak power of the input pulse P_0 is $4P_{\mathrm{cr}}$. As we see in Fig. 5, the spatiotemporal dynamics of an intense multi-cycle THz pulse propagating through a normally dispersive medium is qualitatively similar to the corresponding case of a near-IR pulse, which has been discussed in the main text and shown in Fig. 1.

Funding. Government Council on Grants, Russian Federation (08-08); Russian Foundation for Basic Research (19-02-00154 A); Office of Naval Research (N00014-19-1-2247); Natural Sciences and Engineering Research Council of Canada.

Acknowledgment. R. W. B. acknowledges the support of the Canada Excellence Research Chairs Program, an NSERC award. R. W. B. and S. C. gratefully acknowledge financial support by the U.S. Office of Naval Research.

REFERENCES

1. G. Askaryan, "Effects of the gradient of a strong electromagnetic beam on electrons and atoms," Sov. Phys. JETP-USSR **15**, 1088–1090 (1962).
2. R. W. Boyd, *Nonlinear Optics* (Elsevier, 2003).
3. R. Y. Chiao, E. Garmire, and C. H. Townes, "Self-trapping of optical beams," Phys. Rev. Lett. **13**, 479 (1964).
4. R. W. Boyd, S. Lukishova, and Y. Shen, *Self-focusing: Past and Present* (Springer, 2009).
5. P. Chernev and V. Petrov, "Self-focusing of light pulses in the presence of normal group-velocity dispersion," Opt. Lett. **17**, 172–174 (1992).
6. J. E. Rothenberg, "Pulse splitting during self-focusing in normally dispersive media," Opt. Lett. **17**, 583–585 (1992).
7. D. Strickland and P. B. Corkum, "Resistance of short pulses to self-focusing," J. Opt. Soc. Am. B **11**, 492–497 (1994).
8. G. Luther, J. Moloney, A. Newell, and E. Wright, "Self-focusing threshold in normally dispersive media," Opt. Lett. **19**, 862–864 (1994).
9. A. N. Berkovskii, S. A. Kozlov, and Y. A. Shpolyanskii, "Reducing the self-focusing efficiency of a femtosecond pulse in a transparent medium with dispersion when the number of light vibrations in it is decreased," J. Opt. Technol. **75**, 631–635 (2008).
10. P. Polynkin and M. Kolesik, "Critical power for self-focusing in the case of ultrashort laser pulses," Phys. Rev. A **87**, 053829 (2013).
11. D. E. Laban, W. C. Wallace, R. D. Glover, R. T. Sang, and D. Kielpinski, "Self-focusing in air with phase-stabilized few-cycle light pulses," Opt. Lett. **35**, 1653–1655 (2010).
12. M. Kunitski, M. Richter, M. D. Thomson, A. Vredenborg, J. Wu, T. Jahnke, M. Schöffler, H. Schmidt-Böcking, H. G. Roskos, and R. Dörner, "Optimization of single-cycle terahertz generation in linbo3 for sub-50 femtosecond pump pulses," Opt. Express **21**, 6826–6836 (2013).
13. C. Vicario, B. Monoszlai, and C. P. Hauri, "GV/m single-cycle terahertz fields from a laser-driven large-size partitioned organic crystal," Phys. Rev. Lett. **112**, 213901 (2014).
14. M. Shalaby, C. Vicario, K. Thirupugalmani, S. Brahadeeswaran, and C. P. Hauri, "Intense THz source based on BNA organic crystal pumped at Ti:sapphire wavelength," Opt. Lett. **41**, 1777–1780 (2016).
15. T. Seifert, S. Jaiswal, M. Sajadi, G. Jakob, S. Winnerl, M. Wolf, M. Klaui, and T. Kampfrath, "Ultrabroadband single-cycle terahertz pulses with peak fields of 300 kv cm^{-1} from a metallic spintronic emitter," Appl. Phys. Lett. **110**, 252402 (2017).
16. T. Qi, Y.-H. Shin, K.-L. Yeh, K. A. Nelson, and A. M. Rappe, "Collective coherent control: synchronization of polarization in ferroelectric $pbtio_3$ by shaped THz fields," Phys. Rev. Lett. **102**, 247603 (2009).
17. I. Katayama, H. Aoki, J. Takeda, H. Shimosato, M. Ashida, R. Kinjo, I. Kawayama, M. Tonouchi, M. Nagai, and K. Tanaka, "Ferroelectric soft mode in a $srtio_3$ thin film impulsively driven to the anharmonic regime using intense picosecond terahertz pulses," Phys. Rev. Lett. **108**, 097401 (2012).
18. C. L. Korpa, G. Tóth, and J. Hebling, "Mapping the lattice-vibration potential using terahertz pulses," J. Phys. B **51**, 035403 (2018).
19. L. Pálfalvi, J. A. Fülöp, G. Tóth, and J. Hebling, "Evanescent-wave proton postaccelerator driven by intense THz pulse," Phys. Rev. Spec. Top. Accel. Beams **17**, 031301 (2014).
20. T. Brabec and F. Krausz, "Nonlinear optical pulse propagation in the single-cycle regime," Phys. Rev. Lett. **78**, 3282–3285 (1997).
21. G. Agrawal, *Nonlinear Fiber Optics*, 5th ed. (Academic, 2013).
22. V. P. Kandidov, S. A. Shlenov, and O. G. Kosareva, "Filamentation of high-power femtosecond laser radiation," Quantum Electron. **39**, 205 (2009).
23. G. Fibich and A. L. Gaeta, "Critical power for self-focusing in bulk media and in hollow waveguides," Opt. Lett. **25**, 335–337 (2000).
24. S. A. Kozlov and V. V. Samartsev, *Fundamentals of Femtosecond Optics* (Woodhead, 2013).
25. A. A. Drozdov, S. A. Kozlov, A. A. Sukhorukov, and Y. S. Kivshar, "Self-phase modulation and frequency generation with few-cycle optical pulses in nonlinear dispersive media," Phys. Rev. A **86**, 053822 (2012).
26. S. A. Kozlov and S. V. Sazonov, "Nonlinear propagation of optical pulses of a few oscillations duration in dielectric media," JETP **84**, 221–228 (1997).
27. S. Tzortzakis, L. Sudrie, M. Franco, B. Prade, A. Mysyrowicz, A. Couairon, and L. Bergé, "Self-guided propagation of ultrashort IR laser pulses in fused silica," Phys. Rev. Lett. **87**, 213902 (2001).

28. J. Ranka and A. Gaeta, "Breakdown of the slowly varying envelope approximation in the self-focusing of ultrashort pulses," Opt. Lett. **23**, 534–536 (1998).
29. A. N. Berkovsky, S. A. Kozlov, and Y. A. Shpolyanskiy, "Self-focusing of few-cycle light pulses in dielectric media," Phys. Rev. A **72**, 043821 (2005).
30. K. Dolgaleva, D. Materikina, R. Boyd, and S. Kozlov, "Prediction of an extremely large nonlinear refractive index for crystals at terahertz frequencies," Phys. Rev. A **92**, 023809 (2015).
31. C. L. Korpa, G. Tóth, and J. Hebling, "Interplay of diffraction and nonlinear effects in the propagation of ultrashort pulses," J. Phys. B **49**, 035401 (2016).
32. A. N. Tcypkin, M. V. Melnik, M. O. Zhukova, I. O. Vorontsova, S. E. Putilin, S. A. Kozlov, and X.-C. Zhang, "High Kerr nonlinearity of water in THz spectral range," Opt. Express **27**, 10419–10425 (2019).
33. A. N. Tcypkin, S. E. Putilin, M. C. Kulya, M. V. Melnik, A. A. Drozdov, V. G. Bespalov, X.-C. Zhang, R. W. Boyd, and S. A. Kozlov, "Experimental estimate of the nonlinear refractive index of crystalline ZnSe in the terahertz spectral range," Bull. Russ. Acad. Sci. Phys. **82**(12), 1547–1549 (2018).
34. M. Melnik, I. Vorontsova, S. Putilin, A. Tcypkin, and S. Kozlov, "Methodical inaccuracy of the z-scan method for few-cycle terahertz pulses," Sci. Rep. **9**, 9146 (2019).
35. J. Hebling, M. C. Hoffmann, K.-L. Yeh, G. Tóth, and K. A. Nelson, "Nonlinear lattice response observed through terahertz SPM," in *Ultrafast Phenomena XVI*, P. Corkum, S. Silvestri, K. A. Nelson, E. Riedle, and R. W. Schoenlein, eds., Vol. **92** of Springer Series in Chemical Physics (Springer-Verlag, 2009), pp. 651–653.
36. T. Brabec and F. Krausz, "Intense few-cycle laser fields: frontiers of nonlinear optics," Rev. Mod. Phys. **72**, 545–591 (2000).
37. J. Lu, H. Y. Hwang, X. Li, S.-H. Lee, O.-P. Kwon, and K. A. Nelson, "Tunable multi-cycle THz generation in organic crystal HMQ-TMS," Opt. Express **23**, 22723–22729 (2015).
38. P. Nugraha, G. Krizsán, G. Polónyi, M. Mechler, J. Hebling, G. Tóth, and J. Fülöp, "Efficient semiconductor multicycle terahertz pulse source," J. Phys. B **51**, 094007 (2018).
39. S. W. Jolly, N. H. Matlis, F. Ahr, V. Leroux, T. Eichner, A.-L. Calendron, H. Ishizuki, T. Taira, F. X. Kärtner, and A. R. Maier, "Spectral phase control of interfering chirped pulses for high-energy narrowband terahertz generation," Nat. Commun. **10**, 2591 (2019).